Biochimica et Biophysica Acta 1834 (2013) 2663–2671

Contents lists available at ScienceDirect

Biochimica et Biophysica Acta

journal homepage: www.elsevier.com/locate/bbapap

Identification of catalytically important amino acid residues for enzymatic reduction of glyoxylate in plants

Gordon J. Hoover [a,1], René Jørgensen [b,1,2], Amanda Rochon [a,1], Vikramjit S. Bajwa [a,1], A. Rod Merrill [b], Barry J. Shelp [a,*]

[a] Department of Plant Agriculture, University of Guelph, Guelph, ON N1G 2W1, Canada
[b] Department of Molecular and Cellular Biology, University of Guelph, Guelph, ON N1G 2W1, Canada

ARTICLE INFO

Article history:
Received 10 May 2013
Received in revised form 15 September 2013
Accepted 18 September 2013
Available online 27 September 2013

Keywords:
Arabidopsis thaliana
Glyoxylate reductase
β-hydroxyacid dehydrogenase protein family
Hydroxypyruvate reductase
Photorespiration
Succinic semialdehyde reductase

ABSTRACT

NADPH-dependent glyoxylate reductases from *Arabidopsis thaliana* (*At*GLYR) convert both glyoxylate and succinic semialdehyde into their corresponding hydroxyacid equivalents. The primary sequence of cytosolic *At*GLYR1 reveals several sequence elements that are consistent with the β-HAD (β-hydroxyacid dehydrogenase) protein family, whose members include 3-hydroxyisobutyrate dehydrogenase, tartronate semialdehyde reductase and 6-phosphogluconate dehydrogenase. Here, site-directed mutagenesis was utilized to identify catalytically important amino acid residues for glyoxylate reduction in *At*GLYR1. Kinetic studies and binding assays established that Lys170 is essential for catalysis, Phe231, Asp239, Ser121 and Thr95 are more important in substrate binding than in catalysis, and Asn174 is more important in catalysis. The low activity of the mutant enzymes precluded kinetic studies with succinic semialdehyde. The crystal structure of *At*GLYR1 in the absence of substrate was solved to 2.1 Å by molecular replacement using a previously unrecognized member of the β-HAD family, cytokine-like nuclear factor, thereby enabling the 3-D structure of the protein to be modeled with substrate and co-factor. Structural alignment of *At*GLYR1 with β-HAD family members provided support for the essentiality of Lys170, Phe173, Asp239, Ser121, Asn174 and Thr95 in the active site and preliminary support for an acid/base catalytic mechanism involving Lys170 as the general acid and a conserved active-site water molecule. This information established that *At*GLYR1 is a member of the β-HAD protein family. Sequence and activity comparisons indicated that *At*GLYR1 and the plastidial *At*GLYR2 possess structural features that are absent in *Arabidopsis* hydroxypyruvate reductases and probably account for their stronger preference for glyoxylate over hydroxypyruvate.

1. Introduction

In 1953, Zelitch [1] provided the first report of NAD(P)H-dependent glyoxylate reductase (GLYR, EC 1.2.1.79) activity in crude or partially purified extracts from spinach leaves. Subsequently, evidence from highly purified enzyme preparations of several plant species, as well as organelle fractionation, was obtained for the existence of multiple enzymes with overlapping specificities for glyoxylate versus hydroxypyruvate and NADPH versus NADH, and for distinct cytosolic and plastidial NADPH-dependent glyoxylate reductases that have only low activity for hydroxypyruvate and/or NADH [2–5]. More recently, *Arabidopsis* genes for the two isoforms (cytosolic *AtGLYR1*, GenBank accession no. AY044183, and plastidial *AtGLYR2*, GenBank accession no. AAP42747) were identified using a combination of strategies, including yeast complementation and *in silico* analysis of gene/protein sequence, *in vivo* targeting analysis of green fluorescent protein fusions in tobacco BY-2 suspension cells and *Arabidopsis* plants, and production and kinetic characterization of recombinant proteins [6–10]. Both recombinant *At*GLYRs prefer NADPH over NADH and convert glyoxylate to glycolate, and the *At*GLYR1 has negligible hydroxypyruvate-dependent activity [7,9]. Notably, the two isoforms also convert SSA (succinic semialdehyde) to gamma-hydroxybutyrate, albeit with much lower catalytic efficiency than for glyoxylate [7,9], and the use of single *atglyr1* and *atglyr2* knockouts indicates that they can function in γ-aminobutyrate metabolism during stress [11,12].

Abbreviations: *At*GLYR, *Arabidopsis thaliana* glyoxylate reductase; β-HAD, β-hydroxyacid dehydrogenase; 3-HIBADH, 3-hydroxyisobutyrate dehydrogenase; HPR, hydroxypyruvate reductase; 6-PGDH, 6-phosphogluconate dehydrogenase; SSA, succinic semialdehyde; TA, tartaric acid; TSAR, tartronate semialdehyde reductase

* Corresponding author at: Department of Plant Agriculture, Bovey Bldg., Rm 4237, University of Guelph, 50 Stone Rd. E., Guelph, ON N1G 2W1, Canada. Tel.: +1 519 824 4120x53089; fax: +1 519 767 0755.
E-mail address: bshelp@uoguelph.ca (B.J. Shelp).
[1] These authors contributed equally to the paper.
[2] Present address: Department of Microbiology and Infection Control, Statens Serum Institut, 5 Artillerivej, Copenhagen S, DK-2300, Denmark.

1570-9639/$ – see front matter © 2013 Elsevier B.V. All rights reserved.
http://dx.doi.org/10.1016/j.bbapap.2013.09.013

Preliminary analysis of the primary sequence of *At*GLYR1 revealed several sequence elements that are consistent with members of the β-HAD (β-hydroxyacid dehydrogenase) protein family [6]. Identification of the β-HAD family was originally based on similarities in hydroxyacid substrate specificity, oxidative reaction mechanism and conserved glycine-rich sequence elements [13]. The crystal structure of NADP-dependent sheep 6-PGDH (6-phosphogluconate dehydrogenase) in the presence of its substrate 6-phosphogluconate revealed 14 strictly conserved amino acid residues with the potential to be catalytically important [14] (PBD ID 1PGP), and sequence alignments between this protein and NAD-dependent rat 3-HIBADH (3-hydroxyisobutyrate dehydrogenase) enabled identification of a conserved glycine-rich consensus element that includes two residues from the 6-PGDH active site [13]. Directed mutagenesis demonstrated K173 as catalytically crucial and N177 as catalytically important residues in 3-HIBADH. Subsequent mutagenesis and modeling studies enabled identification of additional amino acids as catalytically important residues at the 6-PGDH active site [15–19]. Recently, the crystal structures for *Thermus thermophilus HB8* 3-HIBADH [20] (PDB ID 2CVZ), as well as *Salmonella typhimurium LT2* TSAR (tartronate semialdehyde reductase) [21] (PDB ID 1VPD) and NADPH-dependent *Eubacterium barkeri* 2-(hydroxymethyl)glutarate dehydrogenase [22] (PDB ID 3CKY) became available. This information indicated that TSAR and 2-(hydroxymethyl)glutarate dehydrogenase are also members of the β-HAD family.

In the present paper, information about the β-HAD protein family allowed us to identify catalytically important amino acid residues for glyoxylate reduction in *At*GLYR1 by characterization of the kinetic and binding properties of mutant enzymes. Initially, we had hoped to gain insights into the mechanistic importance of the residues in both glyoxylate and SSA reduction; however, kinetic studies of the mutant enzymes were not possible with SSA since the activities were too low. We were also able to solve the crystal structure of *At*GLYR1 in the absence of substrate (apoprotein; PDB ID 3DOJ) to 2.1 Å by molecular replacement using a previously unrecognized member of the β-HAD family, cytokine-like nuclear factor. This allowed us to model the 3-D structure of the protein with substrate and co-factor. Together, these studies provided support for the importance of these residues and established the basis for including *At*GLYR1 in the β-HAD protein family.

2. Materials and methods

2.1. Expression and purification of recombinant AtGLYR1

Recombinant *At*GLYR2 was produced by amplifying a truncated *AtGLYR2* (Gene ID 838342) cDNA sequence lacking the N-terminal 58 amino acids using primers 5′-GCATCATATGTCTACCAGAGATGAACTTG GAAC-3′ and 5′-GCATGGATCCCTAAGCTTCTCGGGATTTTGC-3′, thereby providing a *Nde*I restriction site on the forward primer and a *Bam*HI site on the reverse primer. The amplified PCR product was cloned into the pET-15b expression vector using *NdeI*/*BamHI* (Novagen, EMD Biosciences Inc., Madison, WI, USA) and sequenced (University of Guelph, Laboratory Services Branch, Guelph, ON, Canada).

The recombinant *At*GLYR1 and *At*GLYR2 were expressed from the isopropyl-β-D-thiogalactopyranoside-inducible pET15b plasmid in *Escherichia coli* BL21 pLysS and purified as described previously [7]. Briefly, post induction (2 h) the BL21 cells were collected by centrifugation, frozen overnight at −20 °C, lysed with lysozyme (1 mg/mL) in buffer (100 mM Tris, pH 8.0, 0.5 mM phenylmethylsulfonyl-fluoride, 1 μg/mL pepstatin A, 2 μg/mL leupeptin) and precipitated with 10% polyethylene glycol 8000 overnight. The precipitate was resuspended in equilibration buffer (50 mM Tris, pH 8.0, 0.5 M NaCl, 20 mM imidazole, 100 μM phenylmethylsulfonyl-fluoride) and loaded on a 4 mL HIS-Select® Nickel Affinity Gel (Sigma) to purify the His_6-tagged protein (as per manufacturer's protocol). The purity of the eluted protein was verified by SDS-PAGE (coomassie stained and western blot) and its concentration was determined with the Bradford assay [7].

2.2. Site-directed mutagenesis of AtGLYR1 active site

The QuickChange site-directed mutagenesis kit (Stratagene) was used to introduce S121A, K170A, K170R, K170E, K170H, N174A, F231A, D239A, T95A mutations into *At*GLYR1 expression plasmid pET15b, using the appropriate primers (see Table S1 in the supplemental material). Mutated plasmids were sent to Genologics (University of Guelph, Laboratory Services Branch, Guelph, ON, Canada) for sequencing (ABI PRISM Sequencer Model 377, PerkinElmer Life Sciences, Foster City, CA, USA).

2.3. Analysis of recombinant protein stability

Purified recombinant proteins were separated by electrophoresis on a 10% SDS-PAGE gel. The separated proteins were detected by immunoblot analysis on nitrocellulose membrane with anti-His monoclonal antibody (Santa Cruz Biotechnology, Santa Cruz, CA) at 1:500 dilution. Blots were developed using alkaline phosphatase-linked secondary antibody at 1:10,000 dilution (goat anti-mouse AP-linked, Sigma, St. Louis, MO) and the alkaline phosphate conjugate substrate kit (Biorad, Hercules, CA).

The purified recombinant enzymes were analyzed by steady-state Trp fluorescence emission scans using PTI QuantaMaster C-61 steady-state fluorimeter (Photon Technology International, London, Ontario, Canada). The temperature of the cuvette was maintained at 22 °C with a circulating water bath. For emission scans, the excitation wavelength was 290 nm and the emission was scanned from 305 to 400 nm with a scan rate of 1.0 nm/s. The excitation and emission wavelengths were set to 2 and 4 nm, respectively. The final concentrations of the native enzyme, denatured native enzyme (using 5 M guanidine-HCl) and the mutant proteins were 60 μg/mL. Each protein spectrum was corrected for the buffer only spectrum and the corrected spectra were normalized. The normalized corrected spectra of the native and mutant enzymes were superimposed to assess differences in shape and emission maxima.

2.4. Enzyme assays

Enzymatic activity of the purified native and mutant *At*GLYR1 enzymes was measured continuously as the oxidation of NADPH using the protocol described previously [7]. Briefly, the reaction mixture consisted of 50 mM 4-(2-hydroxyethyl)-piperazine-1-ethanesulfonic acid, pH 7.8, 10% sorbitol, NADPH, glyoxylate and purified recombinant enzyme. Kinetics with glyoxylate as the varied substrate were conducted at a fixed concentration of NADPH (50 μM); for each enzyme the concentration of glyoxylate was varied to give five to six data points both above and below the K_m. When NADPH was varied, the fixed concentration of glyoxylate was typically 8–10 times the K_m for glyoxylate; the only exception was for the F231A mutant where the maximum concentration of glyoxylate achievable was 2.5 times the K_m. For each enzyme, the concentration of enzyme used was determined to be within the linear range (0.75–2500 nM). One unit of activity equals 1 μmol/min, and all kinetic data were obtained from measurements of initial rate. Measurements were obtained in triplicate at each concentration and typically three to four biological replicates were used. Kinetic data were fit to the Michaelis–Menten equation using non-linear least-squares analysis (SigmaPlot2000, version 6.1; Enzyme Kinetics Module, version 1.0; Systat Software Inc., Point Richmond, CA). A fit was deemed acceptable if it exhibited random residuals, passed the runs test and reached minimum error in all fitting parameters. Kinetics of the native *At*GLYR1 enzyme with lithium β-hydroxypyruvate (Sigma, St. Louis, MO) as the varied substrate were performed essentially as described above for glyoxylate with fixed concentrations of NADPH (50 μM) and enzyme (25 nM). For native *At*GLYR2, kinetics using glyoxylate as a varied substrate were essentially the same as for *At*GLYR1 with the exception that enzyme concentration was 25 nM.

Glyoxylate-dependent quenching of intrinsic tryptophan fluorescence was used to determine the binding constants (K_d). Triplicate reactions were performed in the above described reaction buffer over a concentration range of 0–50 μM glyoxylate in the presence of 1 μM enzyme. Fluorescence measurements were obtained using a Cary Eclipse fluorescence spectrophotometer (Santa Clara, CA) according to the method reported elsewhere [23].

2.5. Crystallization of recombinant AtGLYR1

Purified *At*GLYR1 was desalted and concentrated to 10 mg/mL in 50 mM Tris, pH 7.8, using Microcon-10 centrifugal concentrators (Amicon). Crystallization trials were set up using the sitting-drop vapor-diffusion method at 20 °C. The crystallization conditions were identified from a preformulated commercial screening kit (Hampton Research, Aliso Viejo, CA). The best crystals were obtained by equilibrating a mixture of 2 μL of protein solution and an equivalent volume of reservoir solution (0.2 M calcium acetate hydrate, 20% polyethylene glycol 3350, pH 6.5). Needlelike crystals formed within a few days and grew to diffracting quality size single crystals after approximately six weeks.

2.6. Data collection, structure solution and refinement

Before flash freezing in liquid N_2 the crystals were transferred to paratone-N (Hampton research) for cryo-protection. A native 2.35 Å dataset was collected with our in-house Enraf-Nonius FR571 diffractometer equipped with a rotating Cu anode and a proteum pt135 ccd detector (Bruker AXS). The diffraction images were processed using Proteum2 software package (Bruker AXS). The space group was determined to be body-centered tetragonal with a Matthews coefficient indicating only one molecule per asymmetric unit with a solvent content of 66%. The structure of *At*GLYR1 was solved by molecular replacement using Molrep [24] and the cytokine-like nuclear factor (N-PAC) (PDB entry, 2UYY) as search model. The solution from molecular replacement was used as input to warpNtrace [25], which was able to trace ~70% of the structure. The model was rebuilt in Coot [26] and refined in Refmac5 [27] using TLS at 2.35 Å resolution. Finally, a 2.1 Å data set was collected on the same crystal at beamline 08-ID at the Canadian Light Source in Saskatoon, SK, Saskatchewan. After processing the new data using the HKL2000 software package [28], the model was re-refined at 2.1 Å in Phenix [29] using the new reflection file after extension and transfer of the test set. The buried surface area was calculated by PISA [30].

2.7. Alignments

The multiple sequence alignment was carried out using ClustalW [31] (http://www.ebi.ac.uk) and the output was loaded into the ESPRIPT utility (http://espript.ibcp.fr) to incorporate secondary structure assignment from the *At*GLYR1 crystal structure. The *At*GLYR1 structure was superimposed on the structures of 3-HIBADH-NADPH, 6-PGDH-NAPDH and TSAR-TA using the Brute force alignment command in LSQMAN [32]. Structural figures were prepared in PyMOL [33].

2.8. Statistical analyses

All statistical analyses for the kinetic data were done using SAS 9.1 at the $\alpha = 0.05$ level (SAS Institute, Cary, NC). Data were first checked for homogeneity of variance (Brown and Forsythe's test for homogeneity of variance) and log transformed in cases where equal variance was not observed before being analyzed using Duncan's multiple range (Proc GLM). Unless otherwise indicated, values represent means of three to four biological replicates ± SE.

3. Results and discussion

3.1. Sequence alignment of AtGLYR1 and β-HAD family members

Sequence alignment reveals that the amino acid identity among *At*GLYR1, two known members of the β-HAD family (3-HIBADH and TSAR), and N-PAC ranges from 23 to 48% (Fig. 1). However, the identity between these four proteins and 6-PGDH ranges from only 10 to 19%, and the subunit size is ~30 kD and ~50 kD, respectively. Furthermore, 3-HIBADH, TSAR and *At*GLYR1 all catalyze low energy electron transfer oxidations and reductions [13,14,34], whereas 6-PGDH catalyzes a three-step, high energy oxidative decarboxylation [35]. Also evident from the sequence alignment is that all five proteins share 10 strictly conserved glycines within their primary sequence, contributing to a common structural framework. They contain a rather large conserved primary structure consensus element at their N-terminus that was originally identified by Hawes et al. [13] and later confirmed as the 3-HIBADH signature sequence by Prosite ([LIVMFY](2)-G-L-G-x-[MQ]-G-x(2)-[MA]-[SAV]-x-[SNHR]) (Prosite (http://expasy.org/prosite/) accession number: PS00895). This element is forgiving in amino acid identity but not in character; therefore, small deviations can be seen in the case of 6-PGDH and N-PAC.

3.2. Kinetic characterization of putative active-site mutants of AtGLYR1

Based on earlier studies of 3-HIBADH, 6-PGDH and TSAR [34,36]; see also references above), five putative active-site residues and a characteristically conserved T95 residue were identified in *At*GLYR1 (Fig. 1) and replaced with Ala (S121A, K170A, N174A, F231A, D239A, T95A). Lys170 was also replaced with Arg, Glu or His. The mutant enzymes, like the native *At*GLYR1 [7], could be highly expressed in *E. coli* and then extracted and purified to homogeneity (see Fig. S1A in the supplemental material). Trp emission scans revealed that the emission maximum and the shape of the fluorescence scan were similar for mutant and native enzymes (see Fig. S1B in the supplemental material), indicating that stability and probably folding were unaffected by the introduced mutations.

We had planned to investigate the importance of the various residues in the reduction of SSA, as well as glyoxylate; however, the activities of the mutant enzymes with SSA were generally too low for kinetic studies. Thus, we focused on the glyoxylate-dependent reaction; the kinetic and binding parameters are summarized in Tables 1 and 2. The native enzyme displayed values for catalytic efficiency (*k*cat/*K*m) and affinity (*K*m) for glyoxylate and NADPH of 3407 s^{-1} mM^{-1}, 18 μM and 3.4 μM, respectively, as determined with the use of a microplate reader. These values are in agreement with previous data obtained with a double beam spectrophotometer, which demonstrated a much higher catalytic efficiency and affinity for glyoxylate (2870 s^{-1} mM^{-1}, 4.5 μM) than for SSA (11.6 s^{-1} mM^{-1}, 870 μM), as well as a comparable affinity for NADPH (2.2 μM) [7]. Here, even less favorable values were obtained for these kinetic parameters using hydroxypyruvate (*k*cat/Km = 0.232 s^{-1} mM^{-1} and K_m = 6.1 mM), indicating that hydroxypyruvate is a very poor substrate for *At*GLYR1. These biochemical properties are consistent with those reported in early studies of NADPH-dependent glyoxylate reductase activity from tobacco and spinach [2,3,5].

There was a four- to 70-fold range in the K_m and k_{cat}/K_m values for NADPH across the enzymes tested (Table 1), whereas the values for glyoxylate varied by 800- to 18,000-fold (Table 2), indicating that interactions with glyoxylate were dramatically more sensitive to the putative active-site mutations. For the K170A mutant, glyoxylate turnover could not be detected even at elevated enzyme and substrate concentrations, and the K_d value was comparable to that in the native enzyme (Table 2), indicating that this Lys is crucial for catalysis. The k_{cat} values for glyoxylate in the K170R and K170E mutants were about three and four orders of magnitude, respectively, lower than that for

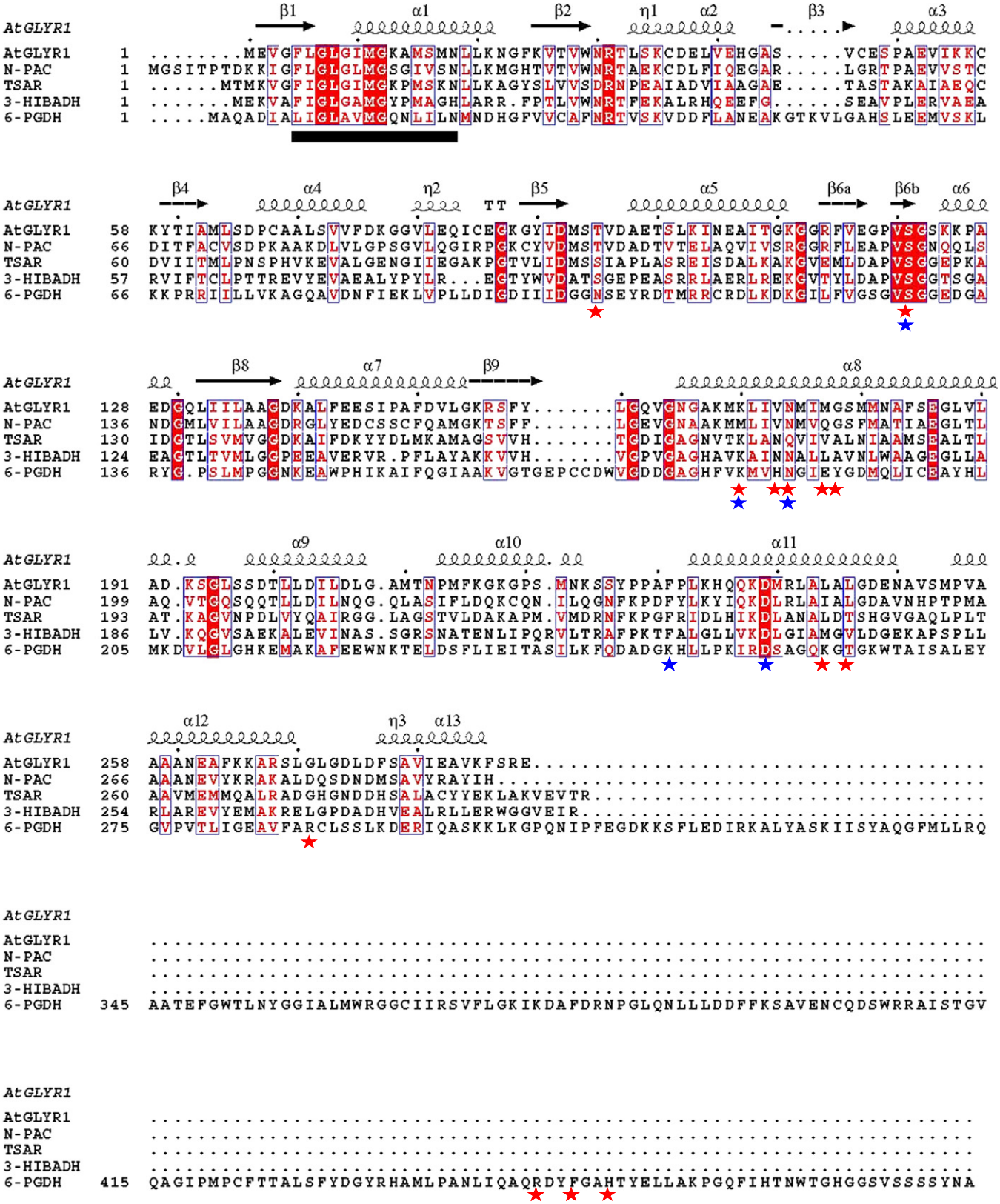

Fig. 1. Primary sequence and secondary structure alignments of native *At*GLYR1 (PDB ID 3DOJ) and N-PAC (PDB ID 2UYY) with the original members of the β-HAD family: 3-HIBADH (PDB ID 2CVZ), 6-PGDH (PDB ID 1PGO), and TSAR (PDB ID 1VPD). The black bar denotes the position of the N-terminal Prosite 3-HIBADH signature sequence [LIVMFY](2)GLGx[MQ]Gx(2)[MA]-[SAV]x[SNHR]. The blue stars indicate the positions of the *At*GLYR1 active-site consensus sequence Sx(48)Kx(3)Nx(56)Fx(7)D. The red stars indicate the positions of the 6-PGDH active-site consensus sequence Nx(25)Sx(54)Kx(2)HNx(2)EYx(68)KxTx(24)Rx(158)Rx(2)Fx(2)H [7]. The numbering for 6-PGDH in the above alignment is one amino acid higher than the numbering related to the 1PGO entry, wherein the sequence starts at the Ala, which corresponds to the second amino acid in the alignment above.

Table 1
Kinetic parameters for recombinant native and mutant *At*GLYR1s with NADPH. Values represent the mean of two–four biological replicates ± SE. Shared letters within each column indicate no significant difference between samples as determined by a Duncan's multiple range test (when necessary, data were log transformed in order to ensure equal variance).

*At*GLYR1	k_{cat}/K_m (s^{-1} μM^{-1})	K_m (μM)	k_{cat} (s^{-1})
Native	24.3 ± 1.6 b	3.44 ± 0.26 b	84.1 ± 10.4 a
S121A	51.7 ± 6.6 a	1.80 ± 0.07 cd	93.7 ± 14.1 a
N174A	10.9 ± 4.0 c	0.902 ± 0.108 d	9.09 ± 2.38 b
K170A	ND[a]	ND	ND
F231A	4.34 ± 0.55 c	2.04 ± 0.65 cd	9.56 ± 4.26 b
D239A	10.4 ± 2.3 c	2.73 ± 0.67 bc	25.4 ± 2.8 b
T95A	0.779 ± 0.186 d	64.8 ± 3.1 a	51.1 ± 14.5ab

[a] Not detectable at a minimum limit of 120 nM s^{-1}.

the native enzyme; however, there was much less change, if any, in the K_m and K_d values. Furthermore, it was not possible to saturate the reaction for the K170H mutant, even up to a glyoxylate concentration of 200 mM, indicating extremely low interaction with the substrate (data not shown). These findings are in agreement with similar studies on the K183 that is identically positioned within 6-PGDH [14,17].

The S121A, N174A, F231A, D239A and T95A mutants had lower k_{cat}/K_m values for glyoxylate than the native enzyme, but enzymatic activity was not eliminated (Table 2), indicating that these residues are not crucial participants in the catalytic event. Of these mutants, N174A had the lowest k_{cat} (turnover), but the K_d was unaffected, indicating that N174 is more important in catalysis than in binding. F231A and D239A had lower k_{cat} values, and much higher (weaker affinity) or undeterminable K_d values due to their extremely low binding, indicating that these residues are more important in binding than in catalysis. The k_{cat} for S121A was unaffected, whereas the K_d was slightly compromised, suggesting that S121 is more important in binding than catalysis. Similarly, the k_{cat} for T95A was unaffected, but the K_d was undeterminable, indicating that T95 is very important in binding.

3.3. Structure of AtGLYR1 protomer and oligomer

Diffraction data for the *At*GLYR1 crystal without substrate were collected to a maximum resolution of 2.1 Å and the structure was solved by molecular replacement using the phase coordinates from N-PAC, which has a sequence identity of 49%, resulting in high quality electron density maps (see Fig. S2 in the supplemental material). The data reduction and refinement statistics for the model are summarized in Table S2 in the supplemental material. The overall structure of *At*GLYR1 consists of two domains and contains eight β-strands (named β1 through β8) placed in domain I and 13 α-helices (α1 through α13) distributed between the two domains (Fig. 2A). Domain I, with the dinucleotide-binding region, comprises residues 1–165 in the N-terminus. This typical Rossmann fold domain contains two α/β units: a six-stranded parallel β-sheet (β1-β6a) covered by four helices (α1-α5) and followed by a mixed three-stranded β-sheet (β6b-β8) covered by two helices (α6 and α7). Domain II (residues 195–287) consists of only helices (α8–α13) from the C-terminal segment of the protein. The two domains are connected by a long α-helix, α8 (residues 166–194). Like the 3-HIBADH [23], TSAR (PDB ID 1VPD) and N-PAC (PDB code 2UYY) structures, the *At*GLYR1 exists as an apparent tetramer in the crystal. Even though the four enzymes were crystallized in different space groups they all contain a globally identical tetrameric structure (Fig. 2B), which lends further support that these enzymes function as a homotetramer. As carefully described for the 3-HIBADH structure [20] each subunit of the tetramer interacts primarily with two neighboring subunits. The AB subunits show a major buried surface area of 2344.5 $Å^2$ corresponding to 17.4% of the total protomer surface. The AC and AD interface show minor areas of 676.4 $Å^2$ and 294.3 $Å^2$, respectively. Furthermore, the AB interface is essentially mediated by hydrophobic interactions, whereas several hydrogen bonds mediate the AC and AD interface. The tetrameric structure of the *At*GLYR1 oligomer in solution was further confirmed using gel exclusion chromatography (data not shown).

3.4. Structural alignment and NADPH binding in AtGLYR1 and β-HAD family members

The solved crystal structure of *At*GLYR1 without substrate superimposes nicely onto the structures of 3-HIBADH-NADPH, 6-PGDH-NADPH and TSAR-tartaric acid (TSAR-TA) with r.m.s.d. values of 1.5 Å, 1.9 Å and 1.2 Å, respectively, for the C_α atoms (Fig. 3A). This supports the structural relationship of *At*GLYR1 to the β-HAD family. Many NAD(H)/NADP(H)-dependent dehydrogenases contain the Rossmann fold for binding the dinucleotide cofactor [37]; the pyrophosphate group interacts with the *GxGxx*(*G*/*A*) sequence fingerprint motif found in the Rossmann fold. This characteristic glycine-rich fingerprint motif is present in the N-terminal domain (G7–G12, as numbered in *At*GLYR1). We were not successful in crystallizing *At*GLYR1 in the presence of substrate or infusing glyoxylate into the *At*GLYR1 crystal, but the presence of NADPH (from 3-HIBADH-NADPH) and TA (from TSAR-TA) enables identification of residues that are most likely to contribute to substrate binding in *At*GLYR1. Modeling of each substrate into the crystal structure of *At*GLYR1 illustrates a good fit within the proposed binding site (Fig. 3B and C, respectively). Like the 3-HIBADH-NADPH structure, NADPH is most likely bound to the interdomain cleft of the *At*GLYR1 structure. The ADP portion of the cofactor is exposed to the solvent, whereas the nicotinamide ring as well as the TA substrate are shielded from the solvent.

The residues surrounding the NADPH and TA substrates (M11, N30, R31, L64, S121, K170, N174,D239, F231, and T95 as numbered in *At*GLYR1) in the superposition of the four structures are highly conserved and have almost perfectly overlapping positions (Fig. 3D). The potential hydrogen bonds in the apo structure of *At*GLYR1 are listed in Table S3 in the supplemental material and compared to the corresponding bonds in 3-HIBADH-NADPH and TSAR-TA structures. Residues K170, N174 and D239 are positioned within hydrogen bonding distance of

Table 2
Kinetic parameters for recombinant native and mutant *At*GLYR1s with glyoxylate. Values for native and mutant enzymes represent the mean of nine and three–four biological replicates ± SE, respectively. Shared letters within each column indicate no significant difference between samples as determined by a Duncan's multiple range test (when necessary, data were log transformed in order to ensure equal variance). ND, not detectable.

*At*GLYR1	k_{cat}/K_m (s^{-1} mM^{-1})	K_m (mM)	k_{cat} (s^{-1})	K_d (μM)
Native	3407 ± 983 a	0.018 ± 0.002 e	54.6 ± 13.2 a	1.47 ± 0.42 d
S121A	480 ± 17 b	0.181 ± 0.015 c	86.4 ± 6.7 a	15.13 ± 4.02 b
N174A	72.8 ± 12.9 c	0.088 ± 0.011 d	6.06 ± 0.32 c	1.92 ± 0.32 cd
K170A	ND[a]	ND	ND	3.89 ± 1.61 c
K170R	0.86 ± 0.05 e	0.061 ± 0.008 d	0.051 ± 0.004 d	1.41 ± 0.28 d
K170E	0.19 ± 0.03 f	0.033 ± 0.014 e	0.0052 ± 0.0012 e	1.77 ± 0.18 cd
F231A	0.87 ± 0.13 e	12.4 ± 1.70 a	11.0 ± 2.6 c	ND
D239A	7.45 ± 0.53 d	3.00 ± 0.18 b	22.0 ± 0.4 b	183.9 ± 14.49 a
T95A	14.6 ± 2.8 d	4.6 ± 0.16 b	67.8 ± 10.4 a	ND

[a] Not detectable at a minimum limit of 120 nM s^{-1}.

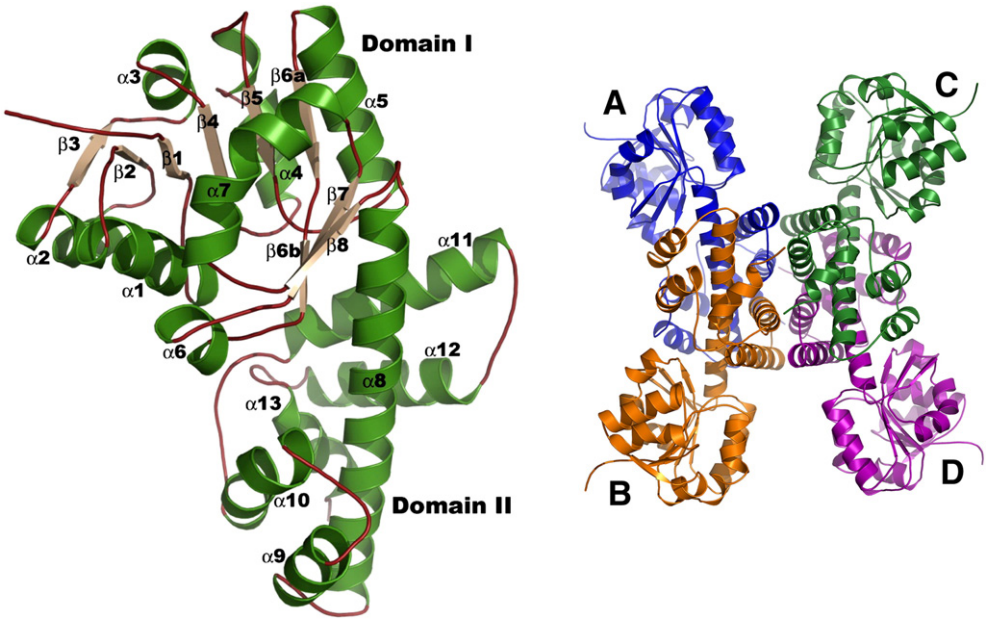

Fig. 2. Ribbon representation of native *At*GLYR1 in the 2.1 Å crystal structure. (A) Protomer with domain and secondary structure assignments; α-helices are shown in green, loops in red and β-strands in light brown. (B) Tetramer as packed in the crystal structure, with subunit A colored in blue, B in orange, C in green and D in purple.

each other, with D239 always hydrogen bonded to a conserved active-site water molecule, as in the 3-HIBADH-NADPH and TSAR-TA structures. These hydrogen-bond interactions could act as a proton relay from the active-site water to K170 via D239 and N174 residues, and then to glyoxylate. Furthermore, the highly conserved water, as seen in the HIBADH holo structure (PDB code 1WP4), could move closer to the catalytically crucial Lys and becomes highly coordinated, giving it the potential to also function as a general acid/base catalyst.

The D239A or N174A substitution in *At*GLYR1 would affect the proton relay between active-site water and active-site Lys and decrease catalytic efficiency and turnover in these mutant enzymes, as is evident from the observed kinetic data (Table 2). For N174, the hydrogen bonding also supports its involvement in orienting K170 during catalysis. The D239A mutant of *At*GLYR1 also had a much weaker binding affinity for glyoxylate than the native enzyme (Table 2), and the binding affinity for the T95A and F231A mutants was below the detection limit (Table 2). However, the k_{cat} values for these three mutants were quite comparable, indicating that T95, F231 and D239 serve a more important role in substrate orientation and docking than in catalysis. All β-HAD family members (except 6-PGDH) have a Phe in their primary sequence, which is identical to the position of F231 in the *At*GLYR1 model. The TSAR model suggests that the steric presence of F231 positions TA towards the cofactor position [21]; a similar relationship most likely exists in *At*GLYR1. The T95 residue of *At*GLYR1 is also characteristically conserved as Ser, Thr or Asn among all β-HAD family members, indicating that a small polar residue is probably required at this position in order to form polar interactions with the substrate molecule. The K_d of the S121A mutant with glyoxylate was slightly compromised; however, the catalytic efficiency was not significantly affected (Table 2), suggesting that the S121 hydroxyl is likely important for recognizing and orienting the substrate.

Overall, these data support the assignment of K170 as a general acid in the acid/base catalytic mechanism of *At*GLYR1. With this in mind, we can speculate on the impact of the K170 mutations on *At*GLYR1 activity (Table 2). The K170A mutation would eliminate the side chain of the Lys residue and therefore any possibility of acid-base catalysis. The side chain of Glu in the K170E mutant would be less likely to accept a proton from the active-site water, probably due to its lower pK and shorter side chain compared to Lys, even though it could form hydrogen-bonding interactions with glyoxylate. The guanidinium group of Arg in the K170R mutant would be capable of accepting a proton from the water molecule, and therefore could function as a general acid by donating a proton to the developing product. However, the catalytic activity with Arg would be lower because it likely has a higher pK in the enzyme environment than does Lys and is therefore a weaker acid [17]. This is not unexpected as the pK of the guanidinium group of Arg is about 12.5 in solution compared to 10.5 for the primary amine group of Lys. With the K170H mutant, there would be a dramatically lower binding affinity for glyoxylate, likely due to the result of steric interference by the imidazole group of the His side chain. We attempted to determine the pK value of the K170 in *At*GLYR1 using nuclear magnetic resonance; however, it was unsuccessful due to the large molecular mass of the *At*GLYR1 tetramer (~120 KDa) and the sorbitol required for enhancing protein solubility/stability in the buffer used. Alternatively, we used the computational pK_a feature in the modeling suite, Molecular Operating Environment 2011.10 (Chemical Computing Group, INC) to calculate the pK_a for K170 in *At*GLYR1 and it was found to be 8.09. However, it must be considered that the *At*GLYR1 (3DOJ) structure does not have bound cofactor or substrate, which will undoubtedly shift the pK_a for K170.

3.5. Comparison of glyoxylate and hydroxypyruvate reductases and potential role during abiotic stress

Photorespiratory flux in plants is typically a function of the ambient levels of CO_2 and O_2 (Fig. 4, [38]). Abiotic stress conditions such as drought and salinity can cause stomatal closure, thereby reducing the internal CO_2/O_2 ratio and resulting in corresponding increases in the oxygenation of ribulose 1,5 bisphosphate, glycolate-2-phosphate, glycolate, and glyoxylate production [39]. In contrast, under hypoxia the photorespiratory pathway would not be expected to generate glyoxylate due to limiting glycolate oxidase activity [40]. All three stresses are likely associated with an elevated NAD(P)H/NAD(P) ratio [11,12], which could limit the mitochondrial conversion of glycine into serine via glycine decarboxylase and where appropriate, cause glyoxylate to further accumulate. The generation of glyoxylate from hydroxypyruvate via the non-photorespiratory serine pathway might also be restricted by unfavorable redox conditions during abiotic stress. Notably, the activities of NAD^+-dependent succinic semialdehyde dehydrogenase and glutamate decarboxylase and NADPH-dependent

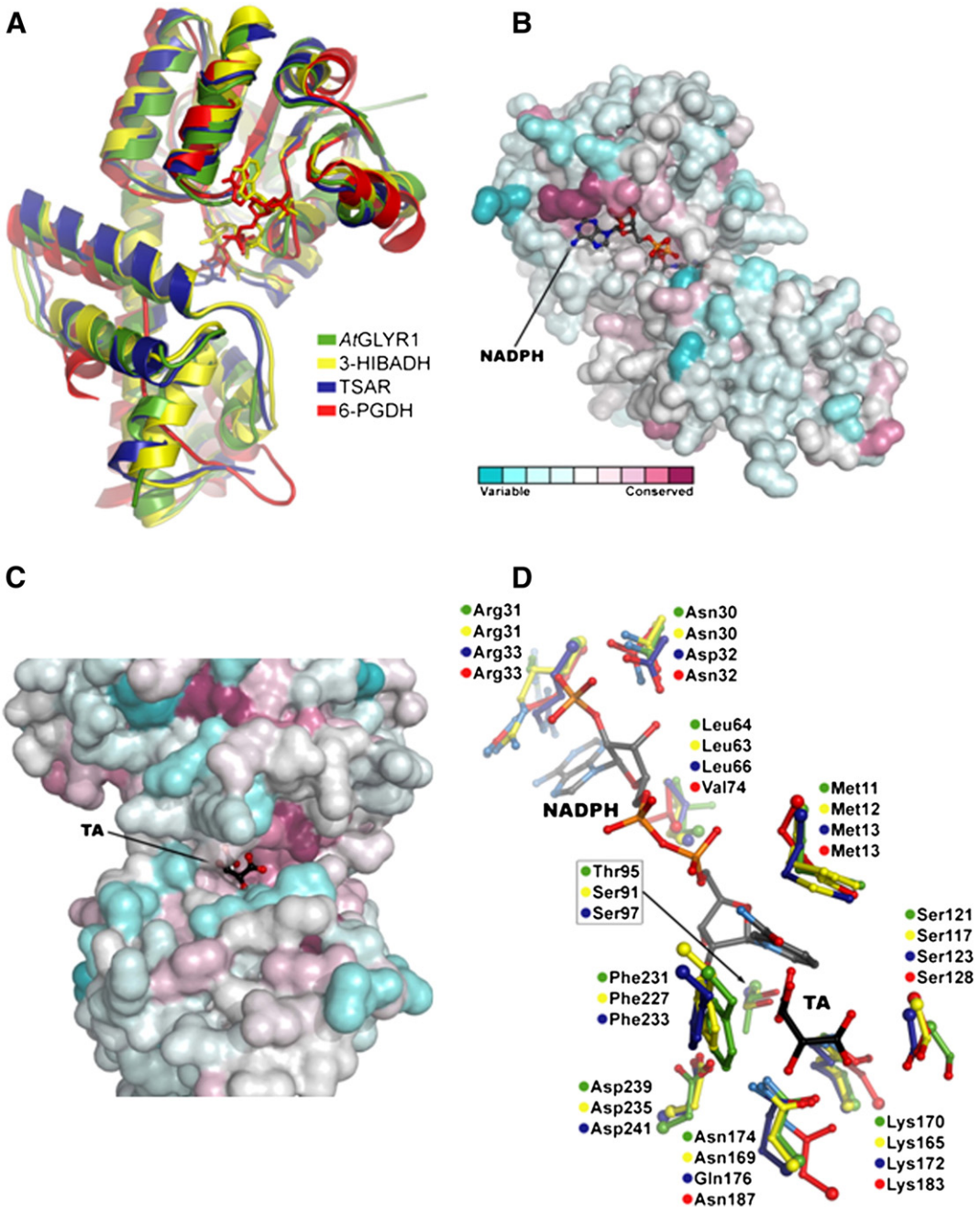

Fig. 3. Structural comparison of native *At*GLYR1 with the β-HAD family. (A) Superposition of the *At*GLYR1 structure (green) with the structures of 3-HIBADH-NADPH (yellow) (PDB ID 2CVZ), 6-PGDH-NADPH (red) (PDB ID 1PGO) and TSAR-TA (blue) (PDB ID 1VPD). Overall ribbon representation of the four structures with the NADPH bound to the 3-HIBADH is shown in yellow sticks, the NADPH bound to the 6-PGDH is shown in red sticks, and the TA bound to the TSAR is shown in blue sticks. (B) Surface representation of *At*GLYR1 with NADPH is shown in gray ball and stick. The surface is colored according to conservation based on the sequence alignment shown in Fig. 2. (C) ~90° rotation of the view as seen in B showing the other side of the binding pocket with the bound TA in black ball and stick. (D) Ball and stick representation of conserved residue side chains important for the catalytic activity of the four structures (colored as in A). NADPH from the HIBADH-NADPH structure is shown in gray and TA from the TSAR-TA structure is shown in black. For clarity the C_α atoms are presented in slightly larger spheres.

SSA reductase activities would be decreased and increased, respectively, resulting in increases in γ-aminobutyrate and γ-hydroxybutyrate production [41,42].

Hydroxypyruvate reductase (HPR) activity is important in the recycling of metabolites derived during photorespiration (Fig. 4). Recent evidence indicated that there are distinct HPR isoforms located in different cellular compartments and with dual substrate specificity: HPR1 is a peroxisomal protein that prefers NADH over NADPH and hydroxypyruvate over glyoxylate; HPR2 is a cytosolic protein that prefers NADPH over NADH but utilizes hydroxypyruvate and glyoxylate similarly; and HPR3 is a plastidial protein that prefers NADPH over NADH and glyoxylate over hydroxypyvruvate (HPR3) [43,44]. Based on substrate specificity, it seems plausible that the NADPH-dependent cytosolic and plastidial *At*GLYRs and *At*HPRs could support the optimum reduction of glyoxylate, as well as hydroxypyruate [12,44]. However, purified recombinant preparations of both *At*GLYR1 and *At*GLYR2 strongly favored the reduction of glyoxylate over hydroxypyuvate, whereas *At*HPR2 and *At*HPR3 had similar maximal activities with both glyoxylate and hydroxypyruvate (Table 3). Comparison of primary sequences indicated that *At*HPR2 and *At*HPR3 were 45% identical to each other at the amino acid level, but only 19–25% identical to *At*HPR1, the NADH-dependent form, and 8–9% identical to the *At*GLYRs

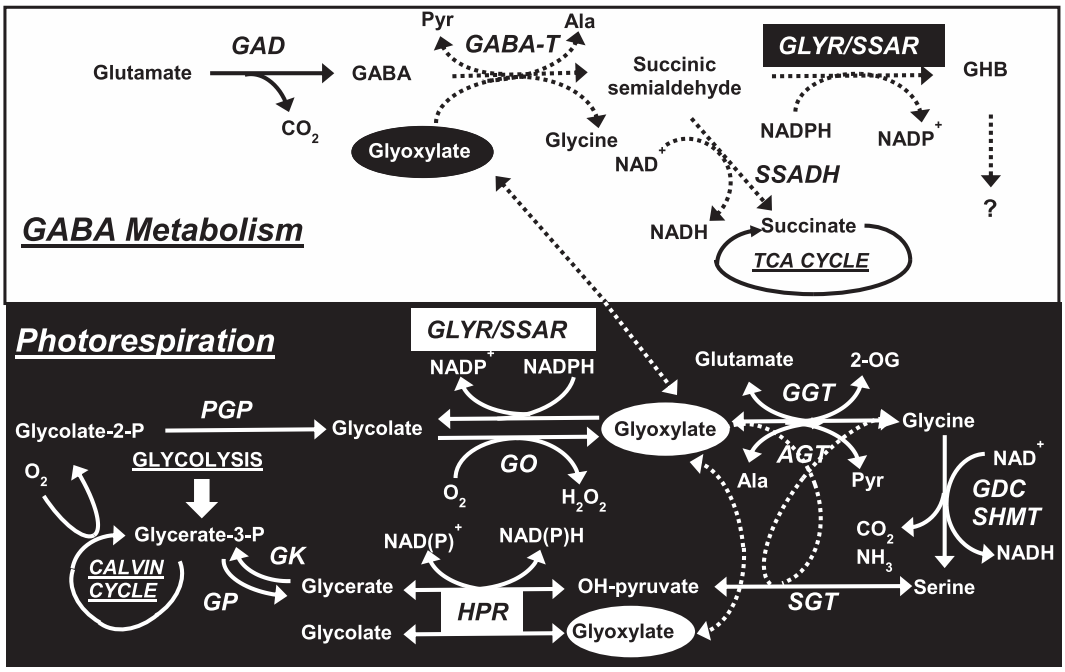

Fig. 4. Enzymatic reduction of glyoxylate via GLYR and HPR activities and potential relationships between photorespiration and γ-aminobutyrate metabolism. Pathway intermediate abbreviations are: Ala, alanine; GABA, γ-aminobutyrate; GHB, γ-hydroxybutyrate; 2-OG, 2-oxoglutarate; Pyr, pyruvate. Enzyme abbreviations are indicated in italics as: AGT, alanine/glyoxylate transaminase; GABA-T, GABA transaminase; GAD, glutamate decarboxylase; GDC, glycine decarboxylase; GGT, glutamate:glyoxylate transaminase; GK, glycerate kinase; GLYR/SSAR, glyoxylate/succinic semialdehyde reductase; GO, glycolate oxidase; GP, glycerate-3-P phosphatase; HPR, hydroxypyruvate reductase; PGP, phosphoglycolate phosphatase; SGT, serine:glyoxylate transaminase; SHMT, serine hydroxymethyl transferase; SSADH; succinic semialdehyde dehydrogenase; TCA, tricarboxylic acid. The primary metabolites and enzymes under consideration are indicated in black/white balloons and squares, respectively. The thick arrow represents reactions of glycolysis, and the question mark represents uncertainty about the fate of GHB [38,39].

(see Fig. S3 in the supplemental material). Furthermore, none of the *At*HPRs contained the active-site residues conserved in *At*GLYR1 and *At*GLYR2, indicating that the sites responsible for reducing glyoxylate differ greatly between the *At*GLYRs and *At*HPRs.

4. Conclusion

Despite low sequence identity, site-directed mutagenesis and structural information revealed that *At*GLYR1 shares common secondary structure, 3-D architecture and functionally important amino acid residues with the β-HAD family, which includes 3-HIBADH, TSAR, 6-PGDH and 2-(hydroxymethyl)glutarate dehydrogenase. The data reported here establishes *At*GLYR1 as the fifth member of the β-HAD family of proteins with known function and as the first family member reported to catalyze the production of either a β-hydroxy (i.e., glycolate from glyoxylate) or a γ-hydroxyacid (i.e., γ-hydroxybutyrate from SSA) [4]. Unfortunately, it was not possible in this paper to assess the mechanistic role of the important amino acid residues in SSA reduction. Further characterization of *At*GLYR1 should contribute to our understanding of the structure-function relations in the small β-HAD protein family and to identification of new family members.

A general acid/base kinetic mechanism is a common feature of oxidoreductase enzymes [45] and previous studies of 6-PGDH have proposed that the oxidation of 6-phosphogluconate to ribulose 5-phosphate utilizes K183 as a general base for deprotonation and stabilization of transition state intermediates [14,17]. In this paper, we proposed that the active site of *At*GLYR1 is an excellent candidate for general acid/base catalysis and addressed the relative kinetic importance in catalysis and binding of five potentially active-site residues (i.e., F231, S121, K170, N174, D239) and a conserved hydroxyl in a Thr residue.

Sequence and activity comparisons indicated that *At*GLYR1 and *At*GLYR2 possess structural features that are absent in the *At*HPRs and that these features could account for their stronger preference for glyoxylate over hydroxypyruvate. On this basis, it is possible that the *At*GLYRs serve a more important role than the *At*HPRs in glyoxylate detoxification and the recycling of reducing equivalents during the

Table 3
Substrate specificity for NADPH-dependent activities of known recombinant native *At*GLYRs and *At*HPRs. Kinetic parameters for *At*GLYR1 with glyoxylate as the substrate were recalculated from Table 2. Kinetic parameters for *At*GLYR1 with hydroxypyruvate as the substrate and for *At*GLYR2 with glyoxylate as the substrate were determined using one typical biological replicate. Values for maximal activity of the *At*HPRs for glyoxylate or hydroxypyruvate were taken from published literature [43,44] and represent the mean of three biological replicates.

Enzyme (subcellular location)	Substrate			
	Glyoxylate		Hydroxypyruvate	
	V_{max} or maximal activity (μmol min^{-1} mg^{-1} prot)	K_m (μM)	V_{max} or maximal activity (μmol min^{-1} mg^{-1} prot)	K_m (mM)
*At*GLYR1 (cytosol)	109	18	2.8	6.1
*At*GLYR2 (plastid)	25	16	–	–
*At*HPR1 (peroxisome)	0.26	–[a]	12	–
*At*HPR2 (cytosol)	4.6	–	5.5	–
*At*HPR3 (plastid)	2.3	–	1.1	–

[a] Data not available.

response to abiotic stress. Recent research demonstrated that the deletion of the NADPH-dependent *At*HPRs influences the photorespiratory phenotype [43,44], but further work is required to assess the involvement of the *At*GLYRs in photorespiration and during abiotic stress. These findings have potential implications for engineering stress resistance in important crop plants.

Acknowledgments

This research was supported by funds from the Natural Sciences and Engineering Research Council of Canada to B.J.S. [grant number 42718-2009] and A.R.M. [grant number 105440-2008], the Canadian Institutes of Health Research to R.J. [fellowship number MFE-78132], and the Ontario Ministry of Agriculture Food and Rural Affairs to B.J.S. [grant number 200131].

Appendix A. Supplementary data

Supplementary data to this article can be found online at http://dx.doi.org/10.1016/j.bbapap.2013.09.013.

References

[1] I. Zelitch, Oxidation and reduction of glycolic and glyoxylic acids in plants. II. Glyoxylic acid reductases, J. Biol. Chem. 201 (1953) 719–726.
[2] I. Zelitch, A.M. Gotto, Properties of a new glyoxylate reductase from leaves, Biochem. J. 84 (1962) 541–546.
[3] L.A. Kleczkowski, D.D. Randall, D.G. Blevins, Purification and characterization of a novel NADPH (NADH)-dependent glyoxylate reductase from spinach leaves. Comparison on immunological properties of leaf glyoxylate reductase and hydroxypyruvate reductases, Biochem. J. 239 (1986) 653–659.
[4] C.V. Givan, L.A. Kleczkowski, The enzymic reduction of glyoxylate and hydroxypyruvate in leaves of higher plants, Plant Physiol. 100 (1992) 552–556.
[5] L.A. Kleczkowski, Kinetics and regulation of the NAD(P)H-dependent glyoxylate-specific reductase from spinach leaves, Z. Naturforsch. 50c (1995) 21–28.
[6] K.E. Breitkreuz, W.L. Allan, O.R. Van Cauwenberghe, C. Jakobs, D. Talibi, B. André, B.J. Shelp, A novel γ-hydroxybutyrate dehydrogenase: identification and expression of an *Arabidopsis* cDNA and potential role under oxygen deficiency, J. Biol. Chem. 278 (2003) 41552–41556.
[7] G.J. Hoover, O.R. Van Cauwenberghe, K.E. Breitkreuz, S.M. Clark, A.R. Merrill, B.J. Shelp, Characteristics of an *Arabidopsis* glyoxylate reductase: general biochemical properties and substrate specificity for the recombinant protein, and developmental expression and implications for glyoxylate and succinic semialdehyde metabolism *in planta*, Can. J. Bot. 85 (2007) 883–895.
[8] G.J. Hoover, G.A. Prentice, A.R. Merrill, B.J. Shelp, Kinetic mechanism of an *Arabidopsis* glyoxylate reductase: studies of initial velocity, dead-end inhibition and product inhibition, Can. J. Bot. 85 (2007) 896–902.
[9] J.P. Simpson, R. DiLeo, P. Dhanoa, W.L. Allan, A. Makhmoudova, S.M. Clark, G.J. Hoover, R.T. Mullen, B.J. Shelp, Identification and characterization of a plastid-localized *Arabidopsis* glyoxylate reductase isoform: comparison with a cytosolic isoform and implications for cellular redox homeostasis and aldehyde detoxification, J. Exp. Bot. 58 (2008) 2545–2554.
[10] S.L.K. Ching, S.K. Gidda, A. Rochon, O.R. Van Cauwenberghe, B.J. Shelp, R.T. Mullen, Glyoxylate reductase isoform 1 is localized in the cytosol and not peroxisomes in plant cells, J. Integr. Plant Biol. 54 (2012) 152–168.
[11] W.L. Alan, J.P. Simpson, S.M. Clark, B.J. Shelp, γ-Hydroxybutyrate accumulation in *Arabidopsis* and tobacco plants is a general response to abiotic stress: putative regulation by redox balance and glyoxylate reductase isoforms, J. Exp. Bot. 59 (2008) 2555–2564.
[12] W.L. Allan, K.E. Breitkreuz, J.C. Waller, J.P. Simpson, G.J. Hoover, A. Rochon, D.J. Wolyn, D. Rentsch, W.A. Snedden, B.J. Shelp, Detoxification of succinate semialdehyde in *Arabidopsis* glyoxylate reductase and NAD kinase mutants subjected to submergence stress, Botany 90 (2012) 51–61.
[13] J.W. Hawes, E.T. Harper, D.W. Crabb, R.A. Harris, Structural and mechanistic similarities of 6-phosphogluconate and 3-hydroxyisobutyrate dehydrogenases reveal a new enzyme family, the 3-hydroxyacid dehydrogenases, FEBS Lett. 389 (1996) 263–267.
[14] M.J. Adams, G.H. Ellis, S. Gover, C.E. Naylor, C. Phillips, Crystallographic study of coenzyme, coenzyme analogue and substrate binding in 6-phosphogluconate dehydrogenase: implications for NADP specificity and the enzyme mechanism, Structure 2 (1994) 651–668.
[15] W.E. Karsten, L. Chooback, P.F. Cook, Glutamate 190 is a general acid in the 6-phosphogluconate dehydrogenase-catalyzed reaction, Biochemistry 37 (1998) 15691–15697.
[16] E. Tetaud, S. Hanau, J.M. Wells, R.W. Le Page, M.J. Adams, S. Arkison, M.P. Barrett, 6-Phosphogluconate dehydrogenase from *Lactococcus lactis*: a role for arginine residues in binding substrate and coenzyme, Biochem. J. 338 (1999) 55–60.
[17] L. Zhang, L. Chooback, P.F. Cook, Lysine 183 is the general base in the 6-phosphogluconate dehydrogenase-catalyzed reaction, Biochemistry 38 (1999) 11231–11238.
[18] L. Li, F.S. Dworkowski, P.F. Cook, Importance in catalysis of the 6-phosphate-binding site of 6-phosphogluconate in sheep liver 6-phosphogluconate dehydrogenase, J. Biol. Chem. 281 (2006) 25568–25576.
[19] R. Sundaramoorthy, J. Iulek, M.P. Barrett, O. Bidet, G.F. Ruda, I.H. Gilbert, W.N. Hunter, Crystal structures of a bacterial 6-phosphogluconate dehydrogenase reveal aspects of specificity, mechanism and mode of inhibition by analogues of high-energy reaction intermediates, FEBS J. 274 (2007) 275–286.
[20] N.K. Lokanath, N. Ohshima, K. Takio, I. Shiromizu, C. Kuroishi, N. Okazaki, S. Kuramitsu, S. Yokoyama, M. Miyano, N. Kunishima, Crystal structure of novel NADP-dependent 3-hydroxyisobutyrate dehydrogenase from *Thermus thermophilus* HB8, J. Mol. Biol. 352 (2005) 905–917.
[21] J. Osipiuk, M. Zhou, S. Moy, F. Collart, A. Joachimiak, X-ray crystal structure of GarR-tartronate semialdehyde reductase from *Salmonella typhimurium*, J. Struct. Funct. Genomics 10 (2009) 249–253.
[22] S. Reitz, A. Alhapel, L.-O. Essen, A.J. Pierik, Structural and kinetic properties of a beta-hydroxyacid dehydrogenase involved in nicotinate fermentation, J. Mol. Biol. 382 (2008) 802–811.
[23] B.K. Beattie, G.A. Prentice, A.R. Merrill, Investigation into the catalytic role for the tryptophan residues within domain III of *Pseudomonas aeruginosa* exotoxin A, Biochemistry 35 (1996) 15134–15142.
[24] A. Vagin, A. Teplyakov, MOLREP: an automated program for molecular replacement, J. Appl. Crystallogr. 30 (1997) 1022–1025.
[25] A. Perrakis, R. Morris, V.S. Lamzin, Automated protein model building combined with iterative structure refinement, Nat. Struct. Biol. 6 (1999) 458–463.
[26] P. Emsley, K. Cowtan, Coot: model-building tools for molecular graphics, Acta Crystallogr. D Biol. Crystallogr. 60 (2004) 2126–2132.
[27] G.N. Murshudov, A.A. Vagin, E.J. Dodson, Refinement of macromolecular structures by the maximum-likelihood method, Acta Crystallogr. D Biol. Crystallogr. 53 (1997) 240–255.
[28] Z. Otwinowski, W. Minor, Processing of x-ray diffraction data collected in oscillation mode, Methods Enzymol. 276 (1997) 307–326.
[29] P.D. Adams, R.W. Grosse-Kunstleve, L.W. Hung, T.R. Ioerger, A.J. Mc-Coy, N.W. Moriarty, R.J. Read, J.C. Sacchettini, N.K. Sauter, T.C. Terwilliger, PHENIX: building new software for automated crystallographic structure determination, Acta Crystallogr. D Biol. Crystallogr. 58 (2002) (2002) 1948–1954.
[30] E. Krissinel, K. Henrick, Inference of macromolecular assemblies from crystalline state, J. Mol. Biol. 372 (2007) 774–797.
[31] M.A. Larkin, G. Blackshields, N.P. Brown, R. Chenna, P.A. McGettigan, H. McWilliam, F. Valentin, I.M. Wallace, A. Wilm, R. Lopez, J.D. Thompson, T.J. Gibson, D.G. Higgins, Clustal W and Clustal X version 2.0, Bioinformatics 23 (2007) 2947–2948.
[32] G.J. Kleywegt, Use of non-crystallographic symmetry in protein structure refinement, Acta Crystallogr. D Biol. Crystallogr. 52 (1996) 842–857.
[33] W.L. DeLano, The PyMOL Molecular Graphics System, DeLano Scientific, Palo Alto, California, USA, 2002.
[34] R.K. Njau, C.A. Herndon, J.W. Hawes, Novel beta-hydroxyacid dehydrogenases in *Escherichia coli* and *Haemophilus influenzae*, J. Biol. Chem. 275 (2000) 38780–38786.
[35] S. Hanau, K. Montin, C. Cervellati, M. Magnani, F. Dallacchio, 6-Phosphogluconate dehydrogenase mechanism: evidence for allosteric modulation by substrate, J. Biol. Chem. 285 (2010) 21366–21371.
[36] R.K. Njau, C.A. Herndon, J.W. Hawes, New developments in our understanding of the beta-hydroxyacid dehydrogenases, Chem. Biol. Interact. 130 (2001) 785–791.
[37] Collaborative computational project, number 4, Acta Crystallogr. D Biol. Crystallogr. 50 (1994) 760–763.
[38] H. Bauwe, M. Hagemann, A.R. Fernie, Photorespiration: players, partners and origin, Trends Plant Sci. 15 (2010) 330–336.
[39] W.L. Allan, S.M. Clark, G.J. Hoover, B.J. Shelp, Role of plant glyoxylate reductases during stress: a hypothesis, Biochem. J. 423 (2009) 15–22.
[40] R. Narsai, K.A. Howell, A. Carroll, A. Ivanova, A.H. Millar, J. Whelan, Defining core metabolic and transcriptomic responses to oxygen availability in rice embryos and young seedlings, Plant Physiol. 151 (2009) 306–322.
[41] B.J. Shelp, G.G. Bozzo, C.P. Trobacher, G. Chiu, V.S. Bajwa, Strategies and tools for studying the metabolism and function of γ-aminobutyrate in plants. I. Pathway structure, Botany 90 (2012) 651–668.
[42] B.J. Shelp, G.G. Bozzo, A. Zarei, J.P. Simpson, C.P. Trobacher, W.L. Allan, Strategies and tools for studying the metabolism and function of γ-aminobutyrate in plants. II. Integrated analysis, Botany 90 (2012) 781–793.
[43] S. Timm, A. Nunes-Nesi, T. P rnik, K. Morgenthal, S. Wienkoop, O. Keerberg, W. Weckwert, L.A. Kleczkowski, A.R. Fernie, H. Bauwe, A cytosolic pathway for the conversion of hydroxypyruvate to glycerate during photorespiration in *Arabidopsis*, Plant Cell 20 (2008) 2848–2859.
[44] S. Timm, A. Florian, K. Jahnke, A. Nunes-Nesi, A.R. Fernie, H. Bauwe, The hydroxypyruvate-reducing system in *Arabidopsis*: multiple enzymes for the same end, Plant Physiol. 155 (2011) 694–705.
[45] C.P. Nicholas, S. Lewis, Fundamentals of Enzymology: The Cell and Molecular Biology of Catalytic Proteins, third ed. Oxford University Press, Oxford, U.K., 1999.